

Compression Causes Expansion and Compaction of the Jammed Polydisperse Particles

Daisuke S. Shimamoto* and Miho Yanagisawa†

*Komaba Institute for Science, Graduate School of Arts and Sciences,
The University of Tokyo, Komaba 3-8-1, Meguro, Tokyo 153-8902, Japan*

(Dated: September 4, 2024)

This study focused on the expansion in polydisperse granular materials owing to mechanical annealing, which involved compression and decompression. Following minor annealing, the polydisperse systems exhibited compaction as well as the systems having uniform-sized particles. However, following extensive annealing, only the polydisperse systems were observed to expand. Pressure history and structure analysis indicated that this expansion results from the size segregation of the particles. We attribute this segregation to particle-size-dependent effective attraction. The results of this study highlight the strong history dependence of the packing fraction and structure in polydisperse particles and reveal a potential-energy-driven segregation mechanism.

The packing fraction of randomly packed particles has been extensively studied from both fundamental and applied perspectives. In idealized systems with frictionless spherical particles, the critical point of the jamming transition or random close packing attracts considerable attention[1–3], and an understanding of its packing fraction has been studied extensively[4–14]. Previous studies have shown that the packing fraction at the jamming point varies depending on the packing protocol and history of macroscopic deformations[4–8]. Beyond the idealized systems, more realistic and complex systems are being studied. The control of the packing fraction is crucial in applications such as soil improvement, transportation efficiency, and material consolidation[15–21].

Many granular materials, such as rubber particles[22], ceramic and metal powders[23, 24], silica particles[20, 21], sand[25, 26], and soils[15–19], exhibit an increase in density following compression and decompression. The increase in packing fraction is known as compaction. Even in numerical simulations focused on frictionless soft-core particles[7, 27–29], a slight compaction is observed following compression and decompression. This compaction is attributed to the optimizations of the configuration, which corresponds to the transition to lower-energy local minima than the original state, and the compression and decompression protocol is referred to as mechanical annealing[7, 28].

Previous studies on compression have focused on compaction and configuration optimization. However, the findings of this study revealed a contrasting phenomenon—expansion in polydisperse systems via extensive mechanical annealing. This expansion challenges the previous understanding of compaction and suggests a novel mechanism for size segregation driven by effective attractive interactions in athermal systems.

This study examined a jammed system comprising polydisperse particles. The particles interacted through purely repulsive forces and only when they were in contact with each other. The interaction potential between the i -th and j -th particles is the following harmonic po-

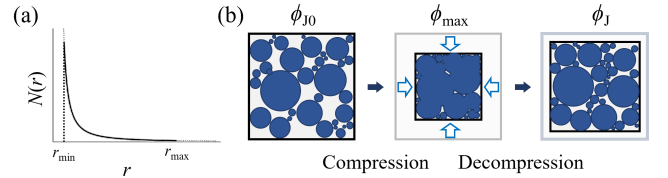


FIG. 1. Schematic showing (a) the power size distribution of spherical particles and (b) their mechanical annealing. Randomly placed particles below the jamming point are compressed isotropically and then decompressed immediately when the packing fraction reaches ϕ_{\max} . The packing fraction immediately after the pressure increases to a finite value during the compression process is defined as ϕ_{J0} , and that immediately before the pressure reaches zero during the decompression process is defined as ϕ_J .

tential:

$$U = \frac{\epsilon}{2} (r_{ij} - d_{ij})^2 \Theta(r_{ij} - d_{ij}), \quad (1)$$

where d_{ij} is the distance between the centers of the i -th and j -th particles, r_{ij} is the sum of their radii, and ϵ is a unit of energy in our simulations. Further, $\Theta(x)$ is the Heaviside step function, defined as $\Theta(x) = 1$ for $x > 0$, and $\Theta(x) = 0$ otherwise.

The distribution of particle radii, $N(r)$, was set to either a power distribution with cutoffs (Fig. 1(a)) or a bidisperse distribution. The power size distribution is expressed as:

$$N(r) = \frac{-a+1}{r_{\min}^{-a+1} - r_{\max}^{-a+1}} r^{-a} \Theta(r - r_{\min}) \Theta(r_{\max} - r), \quad (2)$$

where r_{\min} and r_{\max} are the lower and upper cutoffs of the distribution, respectively, and a is the exponent that characterizes the shape of the distribution. Particles following these distributions were generated using the inverse function method[30] in the same way as we have previously reported[13]. The bidisperse distribution is

an equimolar binary mixture of particles with a size ratio of 1:1.4. The total number of particles was typically set to 4000. For the case of $a = 2.7$, the number of particles was set to 16000 to ensure a size range that spanned two orders of magnitude by generating sufficient amount of the minor component, large particles.

Initial states were prepared by quenching the system from infinite to zero temperature. First, the coordinates of all particles were randomly assigned according to a uniform distribution and placed within a square cell with periodic boundary conditions. The system was then relaxed to a mechanical equilibrium using the FIRE algorithm[31] to minimize energy. Mechanical equilibrium was determined based on the condition that the net force on each particle was below the numerical error. The initial packing fraction was set to be 10^{-2} less than the jamming point.

Mechanical annealing was simulated by increasing and decreasing the packing fraction of the randomly placed particles. Subsequently, the jamming points in the compression process, ϕ_{J0} , and decompression process, ϕ_J , were compared (Fig. 1(b)). The system at the initial state was isotropically compressed in increments of $\delta\phi = 10^{-4}$ until the packing fraction reached the maximum value ϕ_{\max} . After each compression step, the system was relaxed to mechanical equilibrium by minimizing the energy. Smaller increments did not significantly affect the results. Let ϕ_{J0} denote the packing fraction at which the pressure first increased to a finite value during compression. Once ϕ reached ϕ_{\max} , the compression stopped, and decompression began in increments of $\delta\phi = -10^{-4}$. Let ϕ_J denote the packing fraction just prior to the pressure dropping to zero. A trial with a larger ϕ_{\max} indicates stronger mechanical annealing. To reduce the statistical uncertainty, all results were averaged over 10 independent trials.

Figure 2 shows the change in packing fraction before and after annealing, $\Delta\phi = \phi_{J0} - \phi_J$, for the bidisperse and polydisperse systems ($a = 1.8, 2.306, 2.7$), plotted against the maximum packing fraction, ϕ_{\max} . A negative $\Delta\phi$ indicates compaction, whereas a positive value indicates expansion. We first describe the results for the bidisperse system as a reference. In the bidisperse system, $\Delta\phi$ was consistently negative, regardless of ϕ_{\max} . In the region where ϕ_{\max} was small (< 1), $\Delta\phi$ gradually decreased and reached a plateau for ϕ_{\max} of unity. This compaction behavior, reported by Kumar et al.[7], is an example of the history dependence of the jamming point.

Next, we present the results for the polydisperse systems, which were the primary focus of this study. In contrast to the bidisperse system, the polydisperse system exhibited expansion owing to annealing. As an example, below we describe the results for $a = 2.306$ (squares in Fig. 2). For small ϕ_{\max} values ($\phi_{\max} < 1$), the compaction proceeded in a manner similar to that in the bidisperse system, with $\Delta\phi$ decreasing as ϕ_{\max} in-

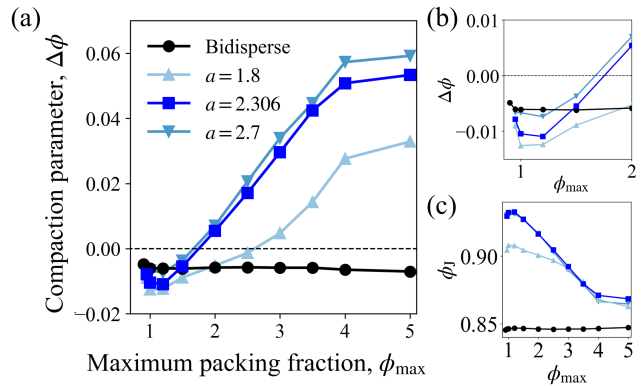


FIG. 2. (a) Plot of $\Delta\phi$ against ϕ_{\max} , and (b) its enlarged plot for $\phi_{\max} < 2$. (c) Plot of ϕ_J against ϕ_{\max} . Each marker corresponds to independent trials with different parameter settings and is not a time series plot of the same trial. The results for Bidisperse systems are indicated as circles, and polydisperse systems are as upward triangles, squares, and downward triangles for exponents $a = 1.8, 2.306, \text{ and } 2.7$, respectively.

creased. The minimum value of $\Delta\phi$, smaller than that in the bidisperse system, indicated more significant compaction. However, once ϕ_{\max} exceeded unity, $\Delta\phi$ began to increase instead of leveling off. Furthermore, when $\phi_{\max} > 1.5$, $\Delta\phi$ turned positive and continued to increase until it plateaued at approximately $\Delta\phi_{\max} = 4$. Compression and decompression alone thus yielded a void fraction range of 6% ($\phi_{\max} = 1.2$) to 14% ($\phi_{\max} = 5.0$). The same tendency of switching $\Delta\phi$ from negative to positive was observed for $a = 1.8$ and $a = 2.7$ (indicated as upward and downward triangles in Fig. 2). These results demonstrated that stronger mechanical annealing of polydisperse systems exhibited a transition from compaction to expansion (or negative expansion).

To elucidate the cause of this negative compaction, we examined changes in the configuration of the packing at the jamming point before and after mechanical annealing. Figure 3 shows the probability distribution of the radius ratio between nearest neighbor particles, obtained from the packings before (Fig. 3(a)) and after (Fig. 3(b)) annealing. The nearest neighbors were determined employing Voronoi Laguerre construction[32, 33]. Before annealing, the broad distribution, indicative of random mixing of large and small particles, contrasted sharply with the post-annealing distribution, where the radius ratio was concentrated near unity (Fig. 3(c)). This concentration indicated size segregation induced by mechanical annealing, as shown in Fig. 3(b).

This size segregation is evident in Fig. 3(b). Before annealing, small particles occupied the voids among the large particles; after annealing, these voids were unoccupied. In terms of the spatial distribution of the particles, the large particles were concentrated around the top and

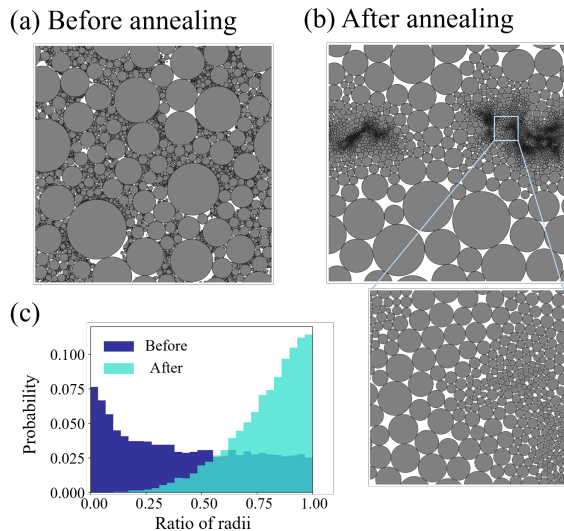


FIG. 3. Example of packing of polydisperse particles ($a = 2.306$) before (a) and after (b) annealing with $\phi_{\max} = 5$. The area enclosed by the white box in (b) is magnified. The darker appearance in (b) is owing to the outlines of accumulated small particles and does not indicate a high local packing fraction. (c) Probability distribution of radius ratios between the particles in the nearest neighbors. The radius ratios are calculated as the smaller radius divided by the larger one.

bottom of the figure. In contrast, the small particles were concentrated around the center of the left and right sides, exhibiting a segregation. The position itself had no physical meaning since the periodic boundary condition was imposed. Owing to segregation, the radii of neighboring particles became more similar.

The reduction in ϕ_J can be attributed to changes in the local structure induced by the size segregation. Numerous studies on the jamming of polydisperse particles[9–14] have shown that systems with uniform size distributions ($\phi_J \simeq 0.84$ [2]) exhibit lower jamming points than polydisperse systems. Size segregation facilitates a more uniform local size distribution, thereby reducing the local packing fraction. Consequently, segregation homogenizes local structure and reduces ϕ_J . This is consistent with segregation-induced expansion specific to polydisperse systems.

Figures 4(a) and (b) show the pressure history during the compression and decompression processes for $\phi_{\max} = 1$ and 5, respectively. During compression, the pressure P increased gradually in most steps, whereas it decreased during decompression. In addition, intermittent pressure drops (indicated by black triangles in Fig. 4(a)) were observed during the compression process. These stress drops corresponded to transitions to lower-energy states with the same packing fraction, caused by plastic deformation with particle replacements[7, 34]. The size segregation observed, as shown in Fig. 3 may be owing to the repeated configuration changes.

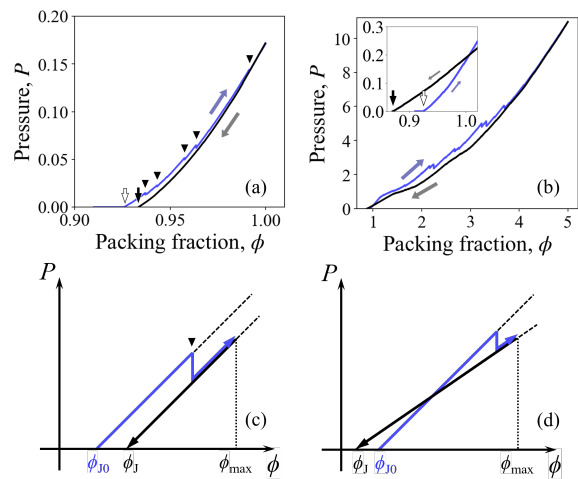


FIG. 4. (a) Pressure history during compression (blue curve) and decompression (black curve) for one of the trials with $\phi_{\max} = 1$. The initial and final jamming points, ϕ_{J0} and ϕ_J , are indicated by white and black arrows, respectively. (b) Pressure history for a trial with $\phi_{\max} = 5$, with a magnified view of the low-pressure region shown in the inset. (c) Schematic of the increase in ϕ_J owing to weak compression. (d) Schematic of strong compression. The effect of the decrease in volumetric modulus exceeds that of stress drops, resulting in a net decrease in ϕ_J .

In the high-pressure region ($\phi > 4$), the absence of stress drops indicated that the configuration changes were completed, and no further replacements occurred. This corresponds to the saturation of $\Delta\phi$ observed in Figure 2(a).

Notably, the strong annealing reduced the pressure slope, as shown in the inset of Figure 4(b). This decrease in slope implied a reduction in the volumetric modulus. The difference in the volumetric modulus was particularly prominent in the low-pressure region ($\phi < 1$), where the system was subject to minimal replacement in the compression process, and was less noticeable in the high-pressure region ($\phi > 4$), where replacement was mostly complete.

The reduction in the volumetric modulus indicated that the replacement and resulting size segregation significantly altered the system’s response to compression. The pressure history thus implied that the replacement caused by strong compression decreased the volumetric modulus, thereby contributing to the observed expansion behavior.

The observed stress drops and changes in the volumetric modulus in the pressure history provide a unified framework for understanding both compaction and negative compaction. Compaction can be explained solely by the stress drops. A stress drop signifies a transition to a lower pressure state with the same packing fraction. Thus, when decompression follows such stress drops, the pressure decreases to zero with less decompression, com-

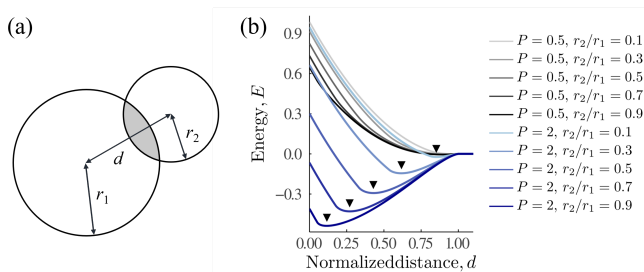


FIG. 5. (a) Schematic of particles in contact, showing the excluded volume reduced by the overlap of them in grey. (b) Effective pairwise potentials for several parameters. Triangles indicate minima. The distance is normalized by $r_1 + r_2$.

pared to the compression phase. Consequently, there is an increase in the jamming point, ϕ_J (Figure 4(c)). This mechanism explains the compaction behavior observed in bidisperse and polydisperse systems with small ϕ_{\max} .

In contrast, only the stress drop cannot explain the negative compaction observed only in the polydisperse systems with large ϕ_{\max} . The strong compression reduces the volumetric modulus, and a lower volumetric modulus necessitates greater decompression before the pressure reaches zero, which reduces ϕ_J (Fig. 4(d)). Upon the strong compression, while stress drops increases ϕ_J , the simultaneous decrease in volumetric modulus counteracts this effect. Negative compaction occurs only when the decrease in ϕ_J owing to the reduced volumetric modulus outweighs the increase from stress drops.

The reduction in the volumetric modulus can be understood by considering the changes in the radius ratio between neighboring particles before and after annealing. Before annealing, large radius ratios between neighboring particles imply that even minor compression can facilitate new contacts with second and more distant neighbors, resulting in a rapid pressure increase. After annealing, size segregation results in a smaller volumetric modulus because the expansion is less likely to increase contact with them. The observed transition from positive to negative $\Delta\phi$ in polydisperse particles should thus be considered as the outcome of this competition between the effects of stress drops and the reduction in volumetric modulus.

We next discuss the effective attractive interactions as a driving force behind size segregation. Above the jamming point, every particle is subjected to pressure from the repulsive forces exerted by surrounding particles. This pressure creates an apparent attractive interaction because reducing the excluded volume through particle overlap reduces the potential energy of neighboring particles. We qualitatively examine the dependence of this effective potential on the particle size ratio and pressure.

Let us first describe the model for the effective potential. The effective potential energy v between two parti-

cles of radii r_1 and r_2 ($r_2 < r_1$) is given by:

$$v = \begin{cases} (r_1 + r_2 - d)^2 - \pi P r_2^2 & r_1 > d + r_2, \\ 0 & d > r_1 + r_2, \\ (r_1 + r_2 - d)^2 - P & \\ \left[r_1^2 \left(\theta - \frac{\sin 2\theta}{2} \right) + r_2^2 \left(\phi - \frac{\sin 2\phi}{2} \right) \right] & \text{otherwise,} \end{cases} \quad (3)$$

where P is the pressure, d is the distance between the particles, and the angles θ and ϕ are defined as:

$$\theta = \arccos \frac{d^2 + r_1^2 - r_2^2}{2dr_1}, \quad \phi = \arccos \frac{d^2 - r_1^2 + r_2^2}{2dr_2}. \quad (4)$$

The first term on the right-hand side of Eq. 3 represents the repulsive potential between the particles. The second term considers the product of the surrounding particles' pressure and the excluded volume reduced by overlap (illustrated by the gray region in Fig. 5(a)). Upon approximating the pressure as hydrostatic, a small inter-particle distance reduces the potential energy owing to the surrounding particles' pressure. Consequently, although the particles interact through a purely repulsive force, an effective attraction emerges owing to this overlap-induced reduction in potential energy.

Next, we discuss the configurations of particles under this effective attraction. Figure 5(b) presents plots of v described in Eq. 3 for various parameter sets, showing the evolution of the interactions under different pressures and particle size ratios. The distance between particles at a mechanical equilibrium corresponds to the value at the minimum of the effective potential v . At low pressures, the interactions remain repulsive (black lines in Fig. 5(b)). However, as the pressure increases, the interactions become effectively attractive, with the potential minima deepening and shifting closer to the origin as the size ratio of the particles, r_2/r_1 , approaches unity (blue lines in Fig. 5(b)). Consequently, while all particles in the system interact through repulsion, particles of similar size effectively attract each other, leading to their accumulation in polydisperse mixtures.

We finally position this effective attractive interaction within the context of known physical interactions. This attraction emerges in an overdamped, gravity-free system, thereby distinguishing it from phenomena driven by gravity, such as the size segregation in the rotating drum experiments[35] or the Brazil nut effect[36, 37]. However, an analogy can be drawn with the depletion interaction, which is an attractive force observed between thermal particles at the microscopic scale. Although the depletion interaction is primarily entropic in nature[38, 39], there are instances wherein an energetic component contributes to the depletion interaction, particularly in systems involving thermal polymers with soft-core repulsive force[40–42]. The attraction discussed in this study, although arising from an energetic rather than an entropic

origin, can be thus considered as a variant of the depletion interaction. This renders it a familiar concept within the broader framework of particle interactions.

In summary, this study discovered the counterintuitive phenomenon of polydisperse particles expanding after compression and decompression. This reduction in density can be understood in two ways. First, the structure of the local packing becomes more homogeneous, and second, the volumetric modulus decreases owing to global size segregation. This expansion contrasted with the typical understanding of compaction, indicating a strong history of dependence on frictionless polydisperse particle packings and facilitating the proposal of a novel size segregation mechanism. The results of this study are expected to enhance the physical understanding of jammed systems composed of polydisperse particles and is applicable to softly interacting systems, such as charged particles, polymers, and magnetic discs, etc.

This research was funded by the Japan Society for the Promotion of Science (JSPS) KAKENHI [grant nos. 23KJ0753 (D.S.) and 23K22459 (M.Y.)] and Japan Science and Technology Agency (JST) Program FOREST [JPMJFR213Y (M.Y.)].

* shimamoto-daisuke806@ecc.u-tokyo.ac.jp

† myanagisawa@g.ecc.u-tokyo.ac.jp; Also at Center for Complex Systems Biology, Universal Biology Institute, The University of Tokyo., Graduate School of Science, The University of Tokyo, Hongo 7-3-1, Bunkyo, Tokyo 113-0033, Japan

- [1] A. J. Liu and S. R. Nagel, Jamming is not just cool any more, *Nature* **396**, 21 (1998).
- [2] C. S. O'Hern, S. A. Langer, A. J. Liu, and S. R. Nagel, Random packings of frictionless particles, *Phys. Rev. Lett.* **88**, 075507 (2002).
- [3] C. S. O'Hern, L. E. Silbert, A. J. Liu, and S. R. Nagel, Jamming at zero temperature and zero applied stress: The epitome of disorder, *Phys. Rev. E* **68**, 011306 (2003).
- [4] A. J. Liu and S. R. Nagel, The jamming transition and the marginally jammed solid, *Annu. Rev. Condens. Matter Phys.* **1**, 347 (2010).
- [5] S. Torquato, T. M. Truskett, and P. G. Debenedetti, Is random close packing of spheres well defined?, *Phys. Rev. Lett.* **84**, 2064 (2000).
- [6] T. Bertrand, R. P. Behringer, B. Chakraborty, C. S. O'Hern, and M. D. Shattuck, Protocol dependence of the jamming transition, *Phys. Rev. E* **93**, 012901 (2016).
- [7] N. Kumar and S. Luding, Memory of jamming–multiscale models for soft and granular matter, *Granul. Matter* **18**, 1 (2016).
- [8] P. Richard, M. Nicodemi, R. Delannay, P. Ribiere, and D. Bideau, Slow relaxation and compaction of granular systems, *Nat. Mater.* **4**, 121 (2005).
- [9] N. Estrada, Effects of grain size distribution on the packing fraction and shear strength of frictionless disk packings, *Phys. Rev. E* **94**, 062903 (2016).
- [10] D. J. Meer, I. Galoustian, J. G. d. F. Manuel, and E. R. Weeks, Estimating random close packing density from circle radius distributions, *Phys. Rev. E* **109**, 064905 (2024).
- [11] M. Hermes and M. Dijkstra, Jamming of polydisperse hard spheres: The effect of kinetic arrest, *Europhys. Lett.* **89**, 38005 (2010).
- [12] R. S. Farr and R. D. Groot, Close packing density of polydisperse hard spheres, *J. Chem. Phys.* **131**, 244104 (2009).
- [13] D. S. Shimamoto and M. Yanagisawa, Common packing patterns for jammed particles of different power size distributions, *Phys. Rev. Res.* **5**, L012014 (2023).
- [14] C. Voivret, F. Radjai, J.-Y. Delenne, and M. S. El Yousoufi, Space-filling properties of polydisperse granular media, *Phys. Rev. E* **76**, 021301 (2007).
- [15] F. W. Taylor and S. E. Thompson, *A treatise on concrete, plain and reinforced: Materials, construction, and design of concrete and reinforced concrete* (J. Wiley & Sons, 1909).
- [16] T. Batey, Soil compaction and soil management—a review, *Soil Use Manag.* **25**, 335 (2009).
- [17] M. F. Nawaz, G. Bourrie, and F. Trolard, Soil compaction impact and modelling. a review, *Agron. Sustain. Dev.* **33**, 291 (2013).
- [18] S. Mooney and W. Nipattasuk, Quantification of the effects of soil compaction on water flow using dye tracers and image analysis, *Soil Use Manag.* **19**, 356 (2003).
- [19] J. Douglas, A. Koppi, and C. Crawford, Structural improvement in a grassland soil after changes to wheel-traffic systems to avoid soil compaction, *Soil Use Manag.* **14**, 14 (1998).
- [20] G. Guiochon and M. Sarker, Consolidation of the packing material in chromatographic columns under dynamic axial compression. i. fundamental study, *J. Chromatogr. A* **704**, 247 (1995).
- [21] M. Sarker, A. M. Katti, and G. Guiochon, Consolidation of the packing material in chromatographic columns under dynamic axial compression ii. consolidation and breakage of several packing materials, *J. Chromatogr. A* **719**, 275 (1996).
- [22] T.-L. Vu and J. Barés, Soft-grain compression: Beyond the jamming point, *Phys. Rev. E* **100**, 042907 (2019).
- [23] A. Cooper Jr and L. E. Eaton, Compaction behavior of several ceramic powders, *J. Am. Ceram. Soc.* **45**, 97 (1962).
- [24] J. T. Black and R. A. Kohser, *DeGarmo's materials and processes in manufacturing* (John Wiley & Sons, 2017).
- [25] G. Mesri and B. Vardhanabhuti, Compression of granular materials, *Can. Geotech. J.* **46**, 369 (2009).
- [26] G. McDowell, On the yielding and plastic compression of sand, *Soils Found.* **42**, 139 (2002).
- [27] T. Kawasaki and K. Miyazaki, Shear jamming and shear melting in mechanically trained frictionless particles, arXiv preprint arXiv:2003.10716 (2020).
- [28] H. Matsuyama, M. Toyoda, T. Kurahashi, A. Ikeda, T. Kawasaki, and K. Miyazaki, Geometrical properties of mechanically annealed systems near the jamming transition, *Eur. Phys. J. E* **44**, 1 (2021).
- [29] P. Chaudhuri, L. Berthier, and S. Sastry, Jamming transitions in amorphous packings of frictionless spheres occur over a continuous range of volume fractions, *Phys. Rev. Lett.* **104**, 165701 (2010).
- [30] L. Devroye, *Handbooks in operations research and management science*, Vol. 13 (Elsevier, 2006) pp. 83–121.

- [31] E. Bitzek, P. Koskinen, F. Gähler, M. Moseler, and P. Gumbsch, Structural relaxation made simple, *Phys. Rev. Lett.* **97**, 170201 (2006).
- [32] K. A. Hart and J. J. Rimoli, Microstructpy: A statistical microstructure mesh generator in python, *SoftwareX* **12**, 100595 (2020).
- [33] J. Matousek, *Lectures on discrete geometry*, Vol. 212 (Springer Science & Business Media, 2013).
- [34] C. E. Maloney and A. Lemaitre, Amorphous systems in athermal, quasistatic shear, *Phys. Rev. E* **74**, 016118 (2006).
- [35] Y. Oyama, The motion of binary particle in a horizontally rotating tube, *Rikagaku Kenkyusho-Iho (Bull. Inst. Phys. Chem. Res.)* **18**, 600 (1939).
- [36] G. F. Smith, L. Hardy, and E. Gard, The segregation of analyzed samples, *Ind. Eng. Chem., Anal. Ed.* **1**, 228 (1929).
- [37] A. P. Brey, H.-M. Ensner, C. A. Kruehle, and I. Rehberg, Reversing the brazil-nut effect: competition between percolation and condensation, *Phys. Rev. Lett.* **90**, 014302 (2003).
- [38] S. Asakura and F. Oosawa, On interaction between two bodies immersed in a solution of macromolecules, *J. Chem. Phys.* **22**, 1255 (1954).
- [39] S. Asakura and F. Oosawa, Interaction between particles suspended in solutions of macromolecules, *J. Polym. Sci.* **33**, 183 (1958).
- [40] L. A. Benton, A. E. Smith, G. B. Young, and G. J. Pielak, Unexpected effects of macromolecular crowding on protein stability, *Biochemistry* **51**, 9773 (2012).
- [41] S. Sukenik, L. Sapir, and D. Harries, Balance of enthalpy and entropy in depletion forces, *Curr. Opin. Colloid Interface Sci.* **18**, 495 (2013).
- [42] L. Sapir and D. Harries, Origin of enthalpic depletion forces, *Biophys. J.* **106**, 671a (2014).